Chapter 5

Application to three years of BALTRAD data

In this chapter, the algorithm scheme is applied to three years (2000-2002) of BALTRAD data. The purpose is to show the distribution of frontal and convective precipitation in several aspects, such as diurnal patterns as well as seasonal and geographical variations. It is focused, beside the overall rainfall attributed to frontal overpasses versus convective precipitation, on its land-sea distribution and the diurnal cycle of both frontal and convective precipitation.

5.1 Data processing

Due to the high temporal resolution of BALTRAD data, massive quantities of BALTRAD precipitation data had to be applied to the algorithm scheme for this examinations. After the application of the algorithm to each 15-minutes slot the pixels of the BALTRAD grid are grouped into either: a) no measurement, b) no rain, c) convective rain or d) frontal rain, respectively. Each pixel which hits or exceeds a given threshold of rain rate was counted as a precipitation event. A statistical evaluation was conducted by analysing the frequency of both precipitation types. The reason for not analysing the rain amount instead lies mainly in the high uncertainty in quantitative estimation of rain amount by dint of radar techniques.

The spatial radar coverage was not stable over the full period (see Fig. 5.1). Some southern areas, partly outside the Baltic Sea catchment region, have observation frequencies of less than 80 percent. Data from this areas are used for textural and geometrical determination of the precipitation type, but are not taken in account for statistical evaluation.

To produce reasonable and comparable long-term statistics, it was necessary to reduce the dimension of 365 (days of a year) x 24 (hours) x 4 (observations per hour) x 815 (first spatial dimension) x 1195 (second spatial dimension) precipitation values into more manageable

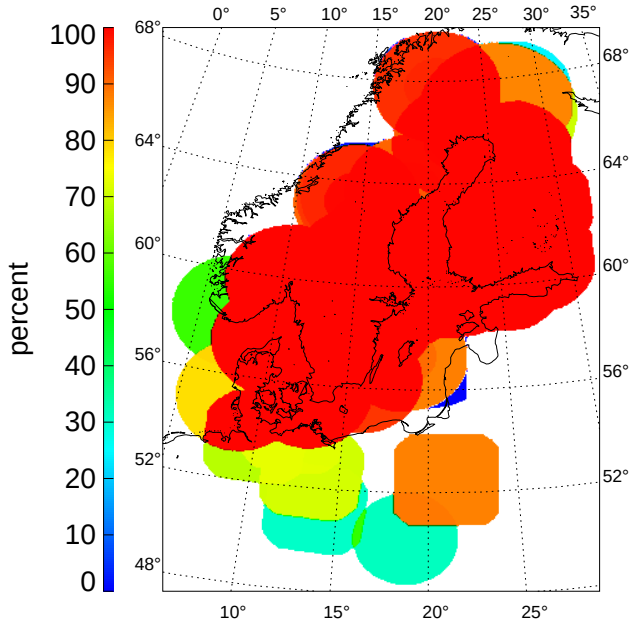

Figure 5.1: Percentage of radar observation coverage in 2000-2002.

functions and parameters. The choice of the type of dimension reduction is linked to the purpose of the investigation and is described as follows:

Geographical patterns: An overview over regional variability is given by maps of geographical distribution of frequency of occurrence of all precipitation events and according to the precipitation type. While the two spatial dimensions are preserved, the temporal dimension vanishes. Each rain event which hits or exceeds a pre-defined threshold of a rain intensity of 0.2 mm/h is taken into account. In this way regional particularities can easily be detected. The spatial resolution is truncated to a resolution of 20 kilometres, because accumulation of radar echoes from a long time period do not provide coherent pattern due to difficulties explained in section 2.1.

Month-daytime analysis: Averaging along the time dimension month-wise and along the local hour of the day gives an overview to seasonal and diurnal variations. The fraction of frontal events were discretely grouped by hour and month. Consequently, the spatial dimensions were totally reduced. The diurnal-year composites of precipitation frequency and rain amount show results for the whole area with no respect to regional effects. Original UTC times were converted to local solar time (LST) assuming

$$LST = UTC + \frac{lon}{15^\circ}. \tag{5.1}$$

where *lon* is the longitude in degrees. LST is grouped to an hourly bin. To give an example, each sample within the period form 0130 LST to 0229 LST represents the 0200 LST time point for an individual month. Values were calculated for each month and each hour by averaging over all available data for this time period, respectively. Thus, the diagrams for one year show interpolated pictures of a 24 (hour of a day) x 12 (months of a year) matrix. This scheme were examined for rain frequency as well as for the fraction of convective events out of all rain events.

Diurnal characteristics Diurnal modulations were investigated by synthesis of the first Fourier harmonic curve. The number of rain events exceeding the threshold of 0.2 mm/h for each pixel were counted according to LST hour according to Eq. 5.1. Subsequently, amplitude and phase shift of the first Fourier wave was calculated as the following:

$$\begin{aligned} F(t) &= A_0 + A_1 \sin(t+\alpha) + residual \\ &= \frac{a_0}{\sqrt{2\pi}} + \frac{a_1 \cos(t)}{\sqrt{\pi}} + \frac{b_1 \sin(t)}{\sqrt{\pi}} + residual \end{aligned} \tag{5.2}$$

with

$$a_0 = \frac{1}{\sqrt{2\pi}} \sum_{x=-\pi}^{\pi} f(x)$$

$$a_1 = \frac{1}{\sqrt{\pi}} \sum_{x=-\pi}^{\pi} f(x) \cos x$$

and

$$b_1 = \frac{1}{\sqrt{\pi}} \sum_{x=-\pi}^{\pi} f(x) \sin x$$

where A_0 corresponds to the daily mean, A_1 the amplitude of the first harmonic, α the phase shift and a_n, b_n are Fourier coefficients. t is the time expressed in radians in the range $[-\pi, \pi]$, with $t = \pi(\frac{LST}{12} - 1)$ as an expression for the local solar time LST in hours. The function $f(x)$ describes the number of events for each time step x. The residual in (5.2) includes the higher-order harmonics of the diurnal variations. The normalised amplitude is defined as the ratio between the first amplitude and the average of daily rain frequency

$$A_n = \frac{A_1}{A_0} \tag{5.3}$$

and can be associated with a significancy estimation of the diurnal variability. To illustrate the meaning of this value, if the normalised amplitude A_n of the diurnal cycle of frontal rain frequency were equal to 0.4, and if higher harmonics were absent, then the probability of frontal rain events would be 1.4 times the daily mean value at the time of the maximum in

the diurnal cycle, and 0.6 times the mean at the time of the minimum. It should be noted that the normalised amplitude can be greater than 1. For example, if there was much less rainfall during the night and much more during daytime, then the normalised amplitude wcould have values even bigger than 2.

The phase shift of the first harmonic refers to the time of the peak t_{max} in the diurnal cycle.

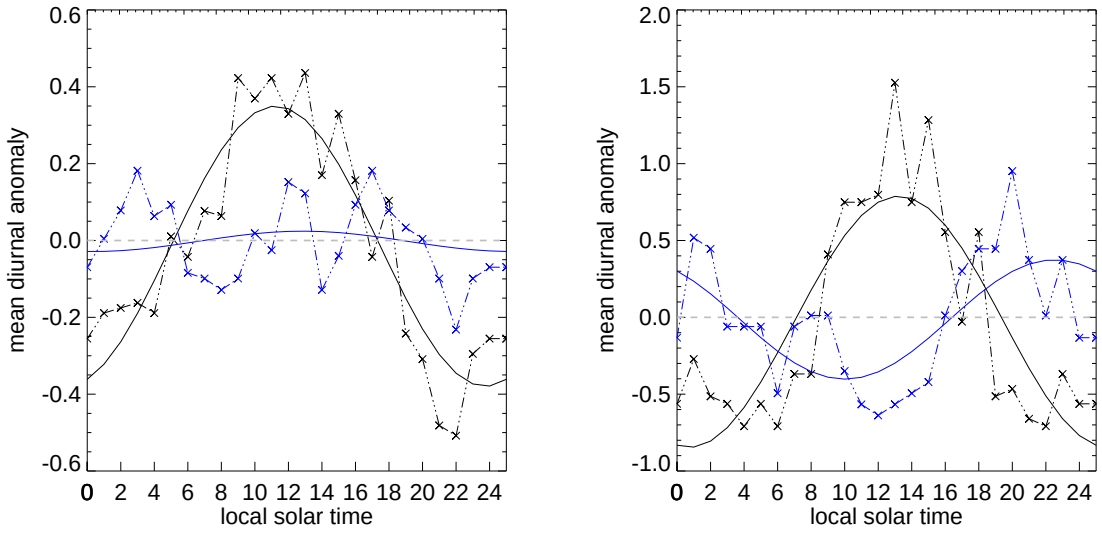

(a) all events (b) convective events

Figure 5.2: Examples of diurnal cycle of overall rain events (left panel) and convective rain events (right panel). Black lines depict a land pixel (longitude: 24.03°, latitude: 62.63°), blue lines sea surface (longitude: 20.11°, latitude: 62.68°). Dashed lines show the average diurnal cycle, solid lines the corresponding first harmonic. Note the different scaling of the y-axis. The corresponding parameters to display in maps are listed in Tab.5.1.

Figure 5.2 shows exemplarily the normalised diurnal cycles of two arbitrarily chosen pixels, one of land surface and the other of sea surface, for all rain events (left panel) and convective rain events (right panel). While the diurnal variability with peaks during afternoon hours dominates over this particular land pixel, the rain frequency variability is weaker at the sea pixel and has a nocturnal maximum. The corresponding values for characterising the diurnal cycle are listed in Tab. 5.1. These calculations were conducted for all season as well as only for summer season.

Time-longitude sections, also referred to as Hovmöller diagrams are a valuable tool to display general patterns over a long time period. In general, Hovmöller diagrams map a scalar quantity to a distance-time space. The scalar variable is averaged along the spatial dimension orthogonal to the spatial dimension plotted in the Hovmöller diagram, usually the

Table 5.1: Parameters to describe the diurnal cycle of the arbitrary chosen example pixels as shown in Fig. 5.2)

.

	longitude	latitude	events	A_n	T_{max}
Land Pixel	24.03°E	62.63°N	all	0.3	11:45
			convective	0.7	13:45
Sea pixel	20.11°E	62.68°N	all	0.1	14:00
			convective	0.4	23:00

x-axis. The ordinate (y-axis) represents the time space. Among other uses, these diagrams have been used to diagnose patterns in the meridional averages for climatological use.

In the case of this study, the procedure is beginning with a time series of frontal/convective classification mapped in the BALTRAD grid. The two spatial dimensions are reduced to one dimension by determination the fraction of frontal pixels within a strip of pixels with identical x-coordinate. Meridional information are totally lost. In this way, the fraction of frontal events becomes one data point in the Hovmöller diagram for each time slot. The BALTRAD projection does not describe an orthogonal longitude/latitude grid, so that the Hovmöller diagrams represents hereby only a "quasi" (approximated) longitude time section. I have decided to not transform the projection in an orthogonal grid, since it is important to preserve the equality of the pixels size. Because frontal systems usually propagating from West to East the number of frontal overpasses and their individual characteristics are well identifiable.

Frontal overpasses statistics Hovmöller diagrams exhibit frontal overpasses in the Baltic area as streaks usually propagating from West to East in forward time direction, e.g. as streaks going from lower left to upper right. An analysis on the images I perform various analysis methods on the Hovmöller diagrams in order to determine duration, zonal distance, zonal velocity as well as number of frontal overpasses. Again, the term *zonal* is to understand as approximation, since Hovmöller domain does not represent a perfect longitude-time section. To identify frontal episodes textural analysis are applied to Hovmöller diagrams.

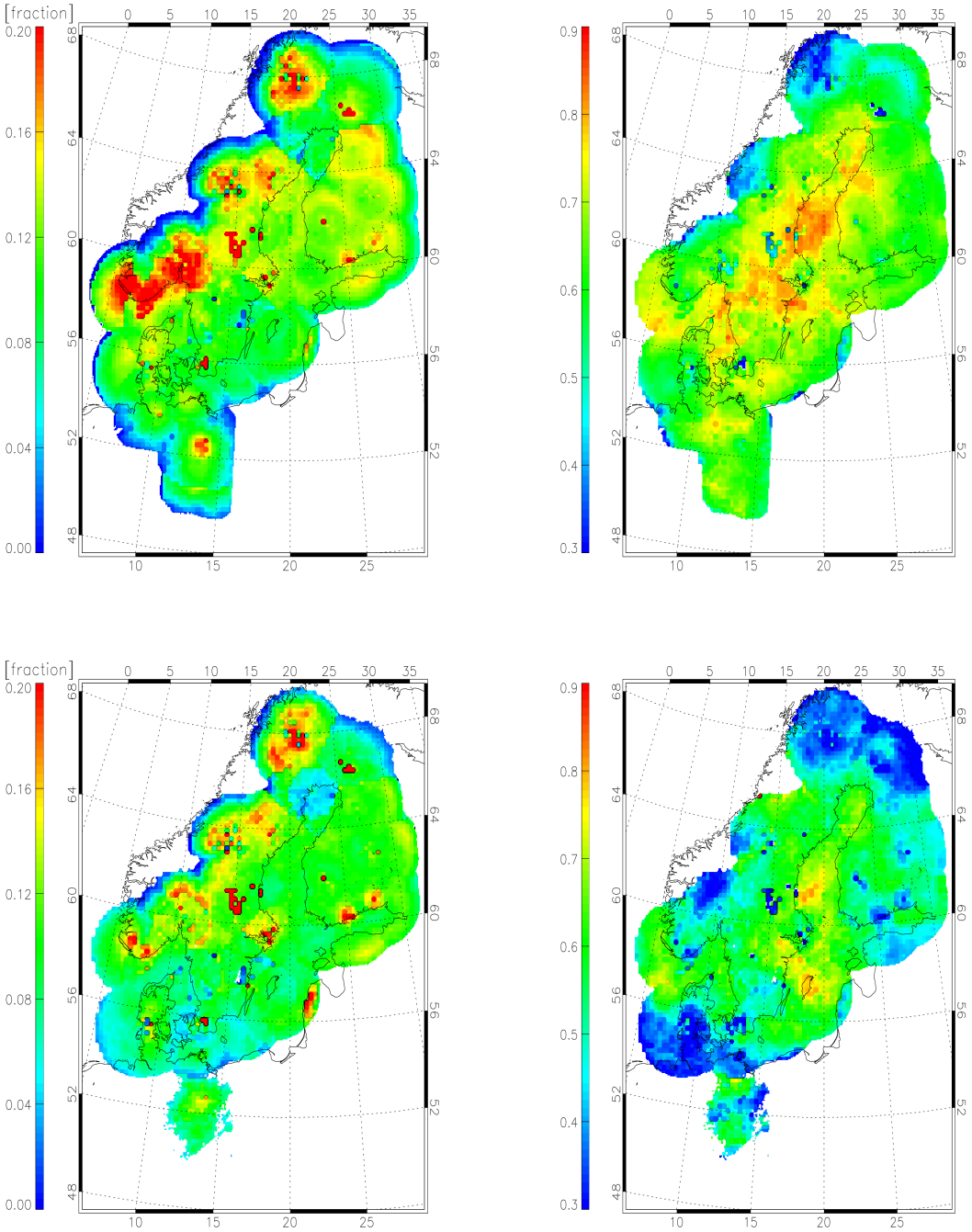

Figure 5.3: Frequency of occurrence of rain events with intensity exceeding 0.2 mmh^{-1} (left panels) and corresponding frontal fraction (right panels). Upper panels show all seasons, lower panels exclusively summer season (June, July, August).

5.2 Results

5.2.1 Overall geographical patterns

This section corresponds to the first item in the data processing section (section 5.1). The geographical patterns of frequency of rain events out of the number of all observations for that pixel and the corresponding frontal fraction are shown in Figure 5.3. Although the spatial resolution was truncated to a lower spatial resolution of 20 kilometres one can easily detect the problems of mapping accumulated rain amounts. The images significantly exhibit regions with apparently falsely identified radar echoes that may be related to remaining ground clutter at the radar sites in Berlin and Lulea (northern Sweden) as well as some border problems between adjacent radar sites south of the Norwegian coast. Typical erroneous features at the border between Doppler and non-Doppler ranges of the Finnish radars could also not be properly corrected. Nevertheless, one can identify typical coherent rainfall patterns of large-scale distribution. For instance, it rains up to 20% of time in the Norwegian mountains due to orographic triggering. In areas without orographic variations, the time fraction ranges from 7% over the southern Baltic Sea and up to 15% in Finland.

The right side panels of Figure 5.3 show the fraction of frontal rain out of overall rain. Besides the already mentioned problems at the two radars in Sweden, there are some typical characteristics: The percentage of frontal events ranges from about 60% to more than 80%. The fraction of frontal precipitation is higher above the sea than over land. This is assumed to be caused by thermally triggered convective precipitation in the warm season. Comparing the overall fraction of frontal rain events with only the summer season in the bottom image is revealing. The percentage of frontal events is less than the yearly average, and the fraction of convective rain increases, especially in heterogeneous land regions (e.g. northern Denmark and central Finland) due to the differential heating of the surface and a resulting increase in convective energy in the summer season.

Table 5.2 summarises the observations after dividing them into regions of Baltic Sea, river drainages and the biggest islands. Not each river catchment was taken into account, but the biggest ones. The first and second column shows the area size and the depth of coverage of the radar composites. The area sizes were calculated based on a catchment mask for the BALTRAD data set and are not necessarily equal with values from other geographical data sources. Note, that the value for the BALTRAD data set coverage in percent indicates the spatial, and not the temporal coverage. This value is calculated by using the largest coverage that occurred during this period of three years. However, there are also temporal gaps in the data set, mainly in the region of the Polish radar sites. The overall spatial coverage is about three fourths of the Baltic sea catchment area. The regions at the Eastern countries still

Table 5.2: Frequency of rain occurrence and fraction of frontal events.

Region	Area size (10 km^2)	BALTRAD cover (%)	Percentage of rain pixels			Fraction of frontal events		
			2000	2001	2002	2000	2001	2002
Baltic Catchment	1721	76.2	10.7	11.3	11.2	0.62	0.64	0.61
Parts of Baltic Sea	415	93.3						
Baltic proper	224	94.3	9.1	10.3	11.2	0.72	0.72	0.68
Bothnian Bay	37	100	10.1	10.6	9.7	0.76	0.77	0.80
Bothnian Sea	82	100	12.6	13.5	11.5	0.80	0.82	0.81
Gulf of Finland	30	100	13.1	16.5	14.0	0.66	0.72	0.69
Gulf of Riga	16	27.5	6.8	6.9	6.0	0.73	0.69	0.70
River drainages								
Ångermanälven	31	100	12.5	12.1	10.2	0.73	0.64	0.57
Göta älv	55	100	12.4	9.7	11.6	0.76	0.72	0.75
Indalsälven	28	100	15.2	14.8	14.7	0.60	0.61	0.40
Kemijoki	53	100	10.9	16.5	15.3	0.55	0.70	0.69
Neva	261	39.1	11.1	11.8	11.4	0.62	0.67	0.65
Oder	119	20.2	5.5	6.4	6.0	0.43	0.47	0.44
Wisla	194	61.5	6.1	5.8	5.5	0.49	0.39	0.43
Islands								
Bornholm	0.62	100	10.8	11.3	12.8	0.53	0.46	0.49
Öland	1.3	100	9.4	11.4	12.0	0.56	0.62	0.63
Gotland	3.0	100	8.9	12.1	10.8	0.80	0.71	0.71

have lacks of radar observations, which explains why the biggest river drainage (Neva) has a BALTRAD coverage of only 39 percent.

The annual overall fraction of frontal events in the Baltic area is approx. 64% and ranges from approx. 50% above islands and land surfaces to 80% in the northern Baltic Sea. The interannual variability is generally weak, especially over sea.

Figure 5.4 shows the dependency of the fraction of frontal events on the rain intensity. Moderate rain events are more likely to be sourced by frontal overpasses than very small as well as intense rain rates. For instance, while the average for convective events is 36 percent, almost half of the pixels with more than 10 mmh^{-1} are initiated by convective processes. A similar trend is observed in rain pixels with very small intensities. This hits the expectation, that convection leads to high rain intensities. The slight increase of convective events probability of very low intensities to those with rain intensity of approx. 1 mmh^{-1} can be explained by occurrence from remaining clutter signals.

5.2.2 Seasonal and diurnal variations

Figures 5.5, 5.6 and 5.7 illustrate the combined seasonal and diurnal cycle of precipitation frequency with intensities exceeding the threshold of 0.2 mmh^{-1} as well as the partition of

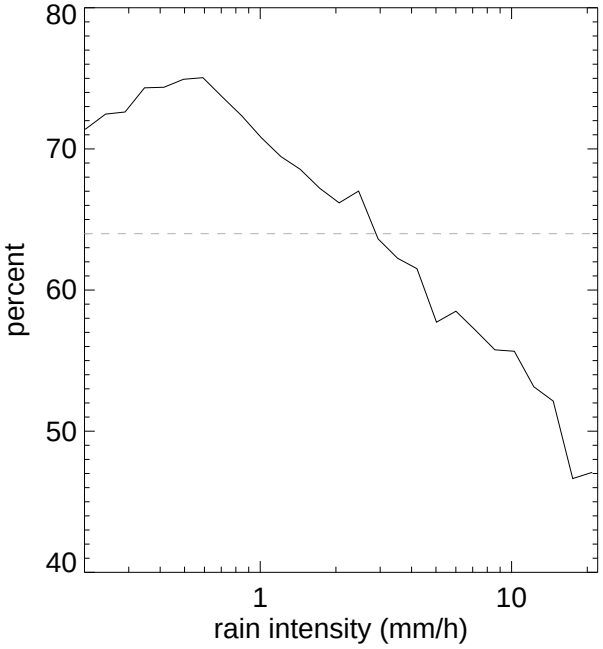

Figure 5.4: Percentage of frontal pixels on overall pixels as a function of rain intensity. The dashed line depicts the overall average for all rain intensity (64 percent)

convective events for 2000 to 2002, respectively. On a first view of the left images, one can discern that no year is like any other with respect to the overall precipitation. In 2002 we notice two significant precipitation periods in spring and in autumn. While 2000 exhibits only one of these periods in autumn, the year 2001 features no strong precipitation period at all. Large precipitation activity coincides with a large number of frontal overpasses with a weak diurnal cycle. The convective fraction decreases in periods with a large number of frontal overpasses to less than 20 percent.

The following points go more in detail of the results:

1. There are periods with high rain frequencies of more than 15 percent (November 2000, February 2002 and November 2002) with a duration of one or two months each. These periods coincided with low convective fractions of less than 20 percent. The diurnal variations are weak in these periods.

2. During summer, rain frequencies have values of about 10 percent, with some values exceeding 13 percent. Warm season is, in general, the time of non-frontal rain and a significant diurnal cycle is observed. Summer rainfall occurs more frequently at daytime (10-18 LST) due to an increased partition of convective rain in afternoon hours. The convective partition in summer at afternoon hours reaches more than 60%.

3. The probability of weak rainfall activity is high during spring and fall. These peri-

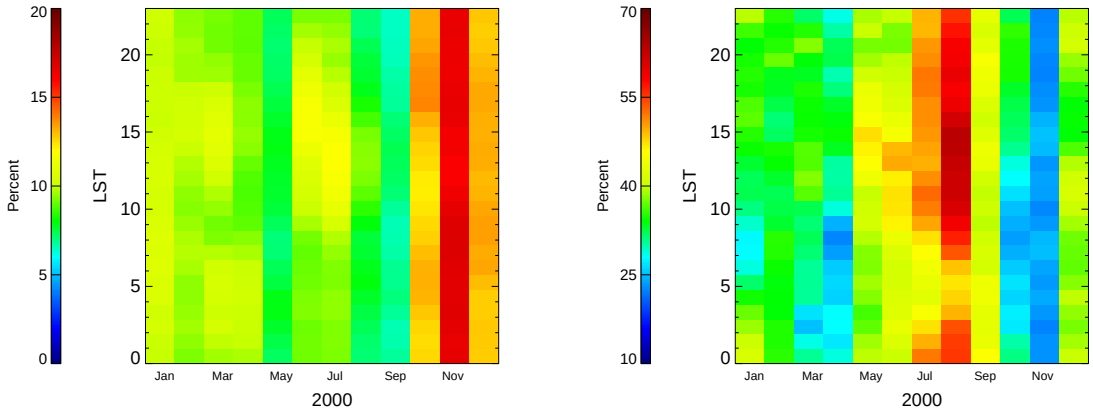

(a) Percentage of time with rain

(b) Convective partition

Figure 5.5: Monthly-diurnal distribution of a.) frequency of precipitation events and b.) the partition of convective rain events out of overall rain events in 2000. LST stands for Local Solar Time.

ods often coincided with a high non-frontal fraction (August and September 2000, September 2002).

4. There are interannual variations in the general pattern. While 2002 had two big precipitation periods, 2000 had only one and 2001 no months with more than 15 percent of time with rain.

5.2.3 Geographical patterns of diurnal cycle parameters

In this section it will be proceeded with describing the bulk spatial characteristics of the diurnal cycle of rainfall according to the type. To get an impression of the regional particularities of diurnal cycle of precipitation images of parameters extracted of the first Fourier harmonic have been generated. Figures 5.8 and 5.9 show the normalised amplitude (i.e. A_n) in Equation 5.3) and phase shift (t_{max} in Eq. 5.2) of the diurnal cycle of precipitation subdivided into frontal and convective categories for the entire time period and for summer season. As mentioned before, the uncorrected features around the radar Lulea (ab. 15°E and 61°N falsify the results in these particular area. Otherwise, the amplitude and the phase maps show a coherent pattern that exhibits the following features:

1. The normalised amplitude of frontal events (right panels) are imperceptible. The highest values are at about 0.2, which means the number of maximal rainfall at the maximal hour is only 1.2 times the daily mean. The phase map exhibits a quite coherent pattern with peak hours during nighttime above Southern Baltic sea and parts of Finland.

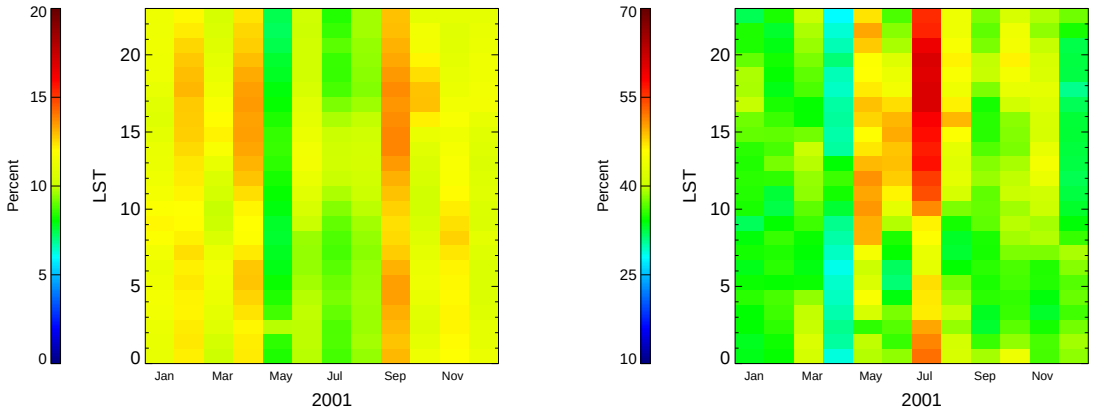

(a) Percentage of time with rain (b) Convective partition

Figure 5.6: Same as Fig. 5.5, but for 2001.

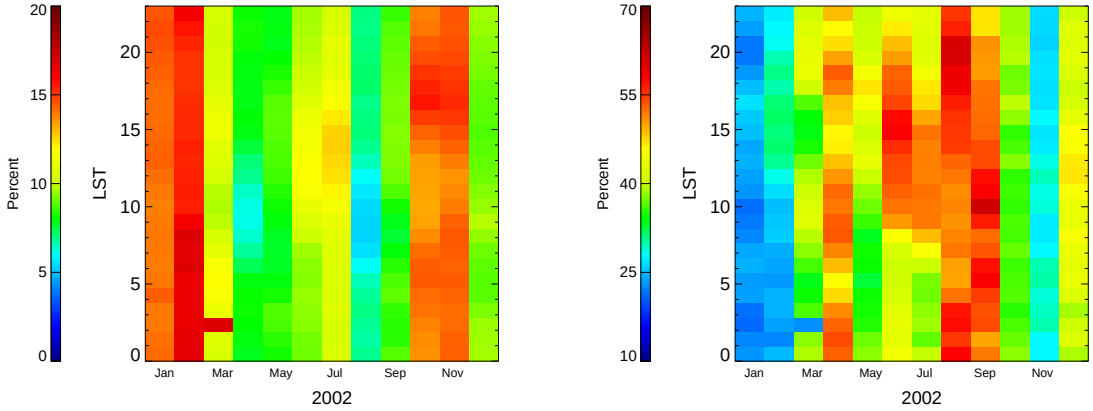

(a) Percentage of time with rain (b) Convective partition

Figure 5.7: Same as Fig. 5.5, but for 2002.

2. The amplitude map of non-frontal events shows a significant diurnal cycle of up to 0.8 for land areas, while the diurnal cycle over sea is weak. Another remarkable feature is the significant land-sea discrimination observed particularly at the Swedish coast.

3. While most of the land pixels display afternoon to late afternoon maxima, sea pixels tend to peak during nighttime. Despite the fact that the amplitude over sea is weak, one can observe exclusively nighttime maxima over the northern part of the Baltic Sea. In Baltic Proper, a region with a couple of islands, the situation is more heterogeneous. Around the German coast numerous pixels with maxima of non-frontal rain occurring during the evening hours (1700-1900 LST) are observable, as well as west of Denmark in parts of North Sea during the morning.

4. There is a significantly stringent land-sea discrimination of amplitude and phase, e.g.

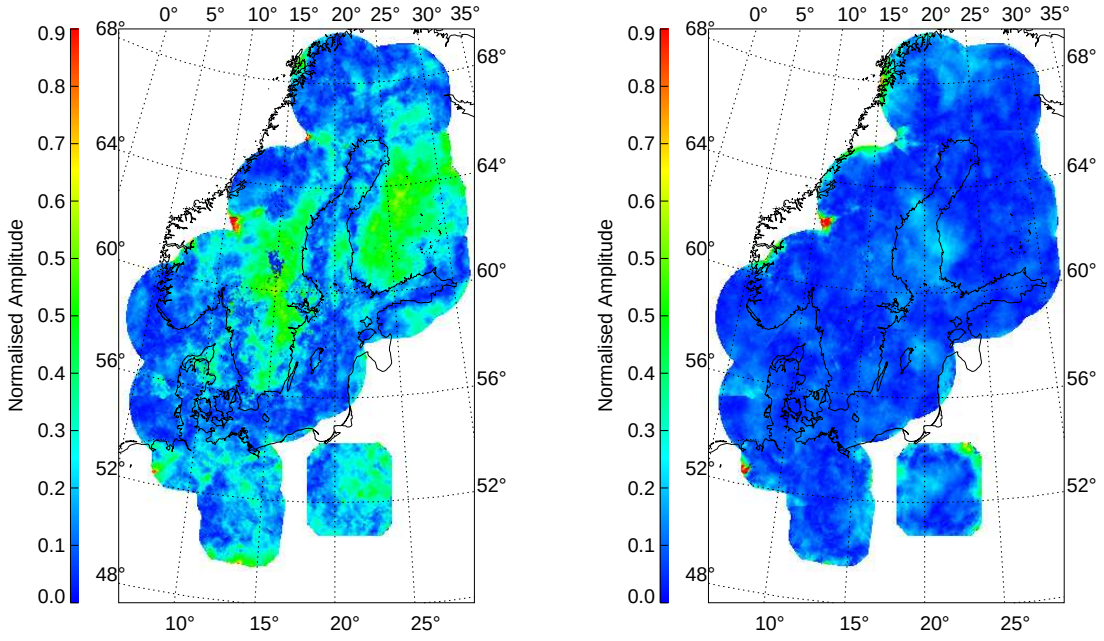

(a) convective events

(b) frontal events

Figure 5.8: Spatial distribution of normalised amplitude A_n of the first harmonic wave in 2000 to 2002 for convective and frontal events.

on the Eastern coast of Sweden.

As mentioned above, summer is the season with the largest convective activity and therefore results of this seasons are very appropriate to highlight the characteristics of geographical aspects of the frontal/convective distribution. Thus, it will be focused on summer in the following. Figs. 5.10 and 5.11 show the same parameters as in Figs. 5.8 and 5.9, but for June, July and August of 2000 to 2002. Some patterns are similar to all season observations, but there are also some significant differences:

1. The diurnal cycle of non-frontal rain events in summer is larger than in the entire period. The amplitude reaches its highest values (more than 1) in some regions in Finland and Sweden. Even though there are almost an equal number of rain events in summer over sea (see Figure 5.10), the amplitude exhibits larger values.

2. The phase pattern is very similar to that of all season. Only the southern parts of the Baltic sea with a daytime peak in all seasons result have nocturnal maxima in the summer. The hour of maximal rainfall over land tends to shift slightly to evening hours. The Bothnian Sea and Bothnian Bay exhibit a west-east distribution of the phase. While in the western parts convective rainfall peaks after midnight (blue colour), the rainfall maxima at the Finnish coast occurs in the late evening shortly before midnight.

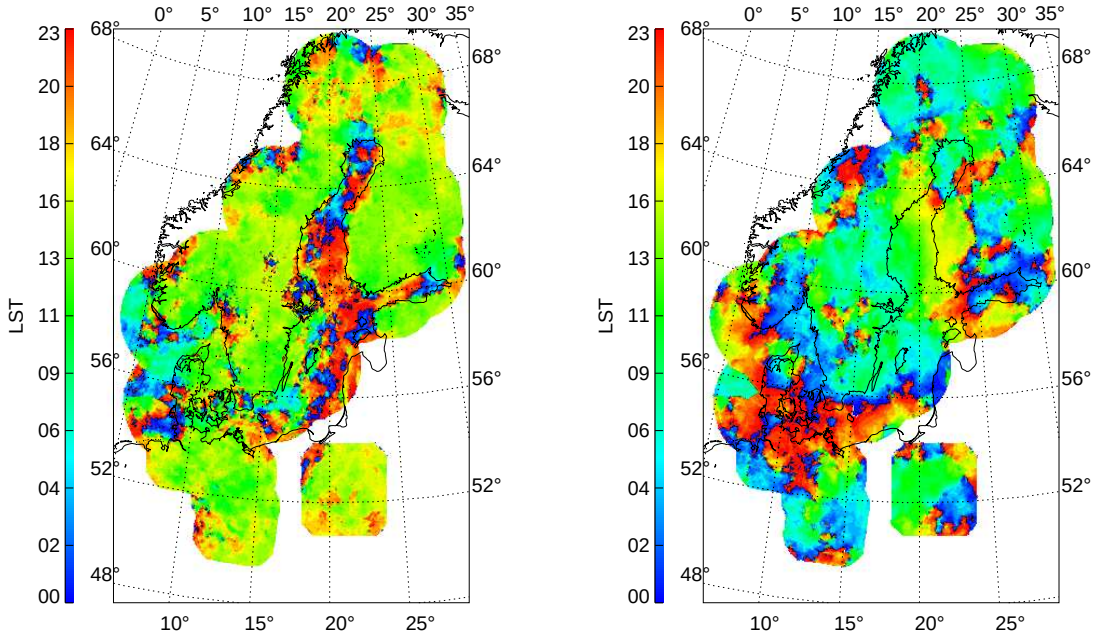

(a) convective events (b) frontal events

Figure 5.9: Spatial distribution of Local Solar Time of the peak of the first harmonic wave for convective and frontal events. Note, that blue and red indicate both nocturnal peaks.

3. In Finland, the middle part of the Baltic Sea around Gotland and Öland, and parts of Northern Germany, the diurnal cycle of frontal rain displays larger significance. In these particular regions, the phase map shows that frontal rainfall peaks with a coherent pattern around noon. In regions with weak amplitude the pattern seems to be randomly distributed.

5.2.4 Frontal overpass statistics

Figure 5.12 illustrates a time-longitude section (*Hovmöller diagram*) of frontal fraction for January 2001. The y axis represents the time axis and ranges from the earliest slot at the lower edge of the image to the latest at the upper edge in an one-hour temporal resolution. Values of x-axis represent the average of frontal fraction in a column of the BATRAD grid. That corresponds to (quasi)-longitude spatial bins from the western (left) to the eastern (right) parts of the BALTRAD domain. If a front goes through the area from west to east a streak with increased frontal fraction appears in the Hovmöller diagram. Particularly pronounced frontal overpasses occur in the beginning of the month around the 3rd January and around the 30th January. A complete compilation of monthly Hovmöller diagrams for three years are given as an appendix (Appendix 7).

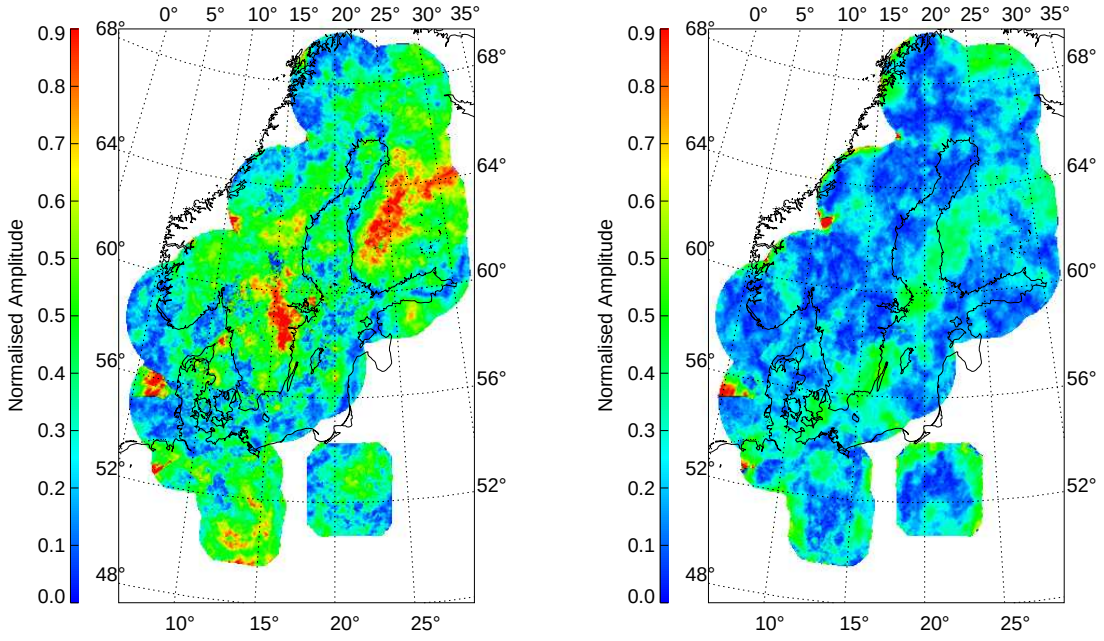

(a) convective events

(b) frontal events

Figure 5.10: Same as Fig. 5.8, but for summer season (June, July, August) 2000-2002.

Although the reduction of one spatial dimension is a loss of information, this kind of data representation is a valuable tool for the evaluation of the characteristics of precipitation. To prove this assumption a cutout of Fig. 5.12 is shown in Fig. 5.13 for the hour 30 (2nd January 06:00 UTC) to hour 63 (3rd January 15:00 UTC). The spatial dimension (x-axis) is hereby given in kilometres distance from the western edge of the domain. To facilate the discussion the corresponding radar images are shown in appendix A.

As mentioned before, Hovmöller diagrams maps a scalar quantity to a distance-time space. In this particular image, x-axis ranges as the distance from the far-left edge of the image from West to East and the y-axis represents the time and runs from the lower part to the upper one. A frontal system, that firstly appears usually in the western part of the area, will be seen at first at the left side of the image. Continuous propagating to East will appear in the Hovmöller domain as a streak from lower left (West and early time) to upper right (East and later time). A linearisation of the propagating path allows the determination of zonal propagation speed for this frontal system. In Figure 5.13 the solid line labelled as number 4 shows such a "fit" for an entire frontal system. The system appears at hour 30 at a distance of 580 km from the western edge of the domain and disappears at hour 61 at a distance of 1500 km. The zonal west-east propagation speed are calculated as following: $v_z = s/t = 1000km/31h \approx 9\ m/s$, where s is the zonal West-East span in kilometres and

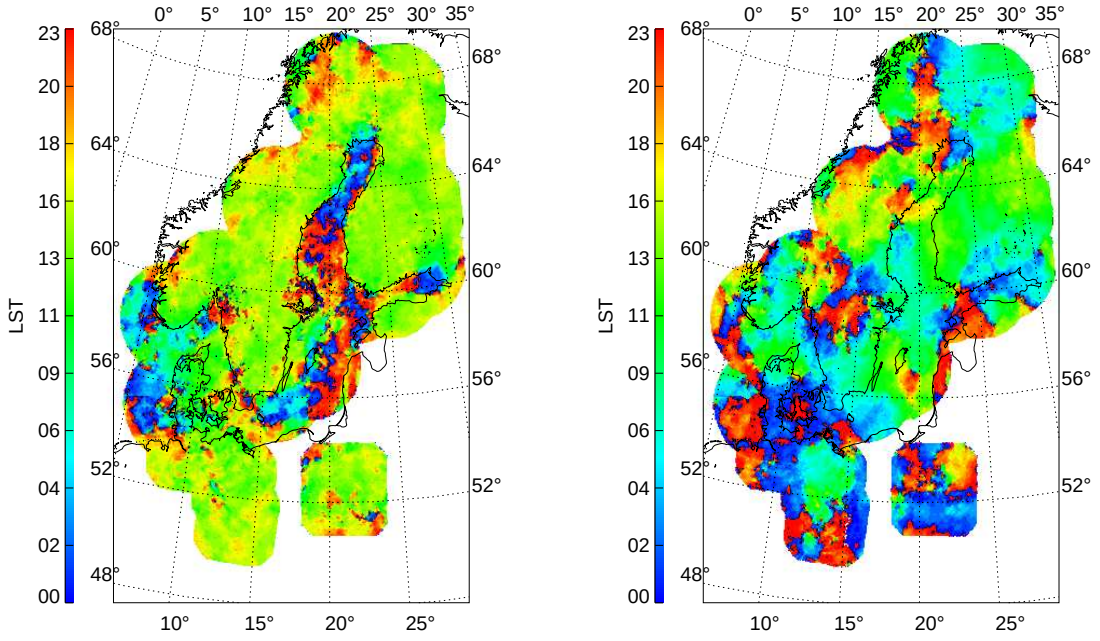

(a) convective events (b) frontal events

Figure 5.11: Same as Fig. 5.9, but for summer season (June, July, August) 2000-2002.

t the duration in hours. More detailed structures are observable within the patterns. Parts of the frontal system labelled with numbers 1, 2 and 3 have particularly high fractions of frontal pixels. Considering the observations at any typical point at distance of 1150 km lead to an interesting interpretation within the Hovmöller diagram: The sequence– high frontal activities at about hour 38, approx. 5 hours with less numbers of frontal pixels and subsequently a second period with high frontal activities – can be interpreted as a sequence of overpasses of a warm front, a warm sector and finally a cold front. The part of the front labelled with 3 can hereby be interpreted as the occlusion of the frontal system starting to occur east of 1150 km. The appendix 7 shows the radar images from hour 29 to hour 59 in two-hours step. This interpretation is not clearly proved, however it seems reliable.

The main attention lies on considering the frontal system as a unit. Herby, the characteristics I wish to determine are the length of the zonal path, zonal propagation speed as well as the duration time. It is obvious, that linear fitting of the streaks of a frontal system in the Hovmöller diagram is not an easy task and is not always objective. To automatically identify frontal events, coherent segments in the Hovmöller space are searched. The first step is similar to that of the algorithm for searching contiguous rainfall areas in Chapter 2: It is to find contiguous areas in the Hovmöller space with pre-defined characteristics. Subsequently other thresholds had to be defined. In order to find the streaks a bundle of calculation steps

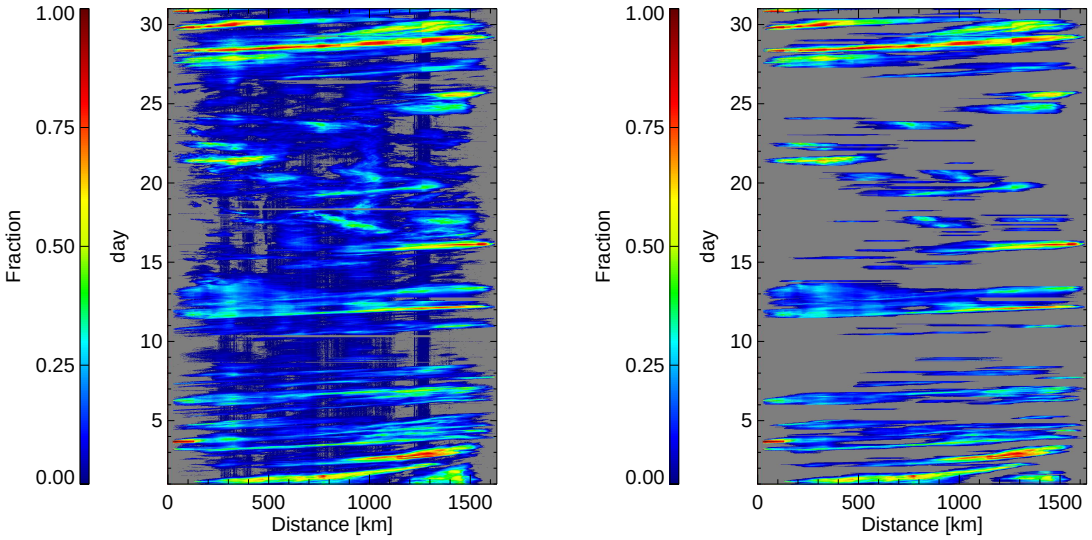

(a) all (b) frontal

Figure 5.12: Hovmöller diagram of January 2000. 8a) shows the fration of overall rain pixels in a quasi-longitude bin. (b) shows the fraction of frontal rain pixels out of all observational pixels in a quasi-longitude bin.

have to be defined in the Hovmöller diagram:

1. Create an Hovmöller diagram H of frontal fraction.

2. Binarize the Hovmöller diagram H, so that each pixel exceeding a pre-defined threshold T_1 gets a label '1'.

3. Find contiguous regions of pixels labelled with '1' in the binarised image using a 8-neighbourhood definition by applying a region growing algorithm.

4. Define a threshold value T_2 for the number of pixels in a contiguous region. Assign every region as an object if the number of pixels in this region exceeds T_2.

5. Define a threshold value T_3 for extension of a contiguous region along the x-axis of H. This value represents the zonal West-East path of the frontal overpass. Keep assigning every object region as an object if the zonal path is larger than T_3, otherwise assign it as background.

6. Define a threshold value T_4 for extension of a contiguous region at along the y-axis of H. This value represents the duration time of the frontal overpass. Keep assigning every object region as an object if the duration time is longer than T_4, otherwise assign it as background.

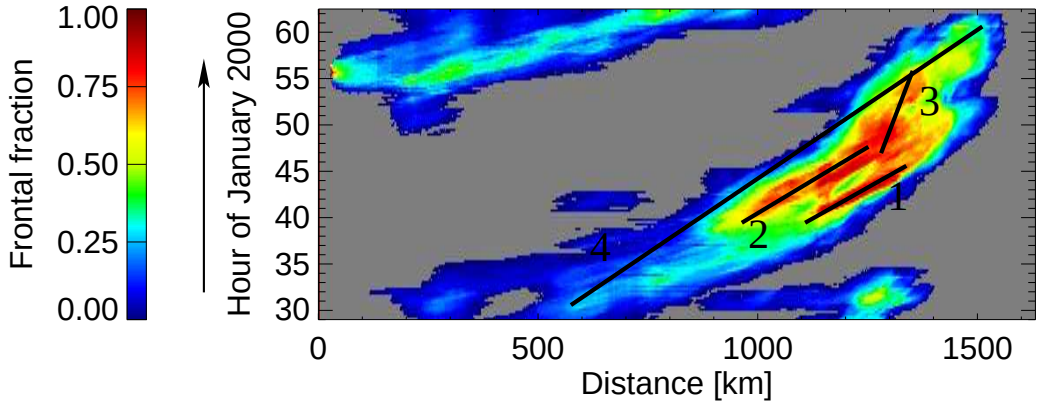

Figure 5.13: Hovmöller diagram for the period of 2nd January 2000 05:00 UTC to 4th January 2000 15:00 UTC. Coherent frontal fraction streaks can be identified in the longitude-time section. The straight, solid lines in the Hovmöller diagram are examples for linear fits of frontal overpasses.

7. Define a threshold value T_5 for the correlation coefficient if each member of an object is seen as a value in a scatterplot diagram. Keep assigning every object region as an object if the correlation coefficient is larger than T_5, otherwise assign it as background.

For producing frontal overpass statistics I have determined two different sets of thresholds. The first one detects the fronts in a more conservative way, the second one has relatively soft criteris. The thresholds are listed in Table 5.3.

Table 5.3: Thresholds definition for detecting frontal overpasses in Hovmöller diagrams.

Threshold number	Description	Unit	Set 1	Set 2
T_1	Frontal fraction	dimensionless	0.2	0.1
T_2	Number of pixels	dimensionless	300	150
T_3	Zonal path	kilometres	550	350
T_4	Duration	hour	15	8
T_5	Correlation coefficient	dimensionless	0.3	0.2

Figures 5.14 and 5.15 show the number of frontal overpasses for each month of the three years from January (J) to December (D) for both sets of thresholds, respectively. Both results resemble each other. While the highest number of frontal overpasses appears in autumn or

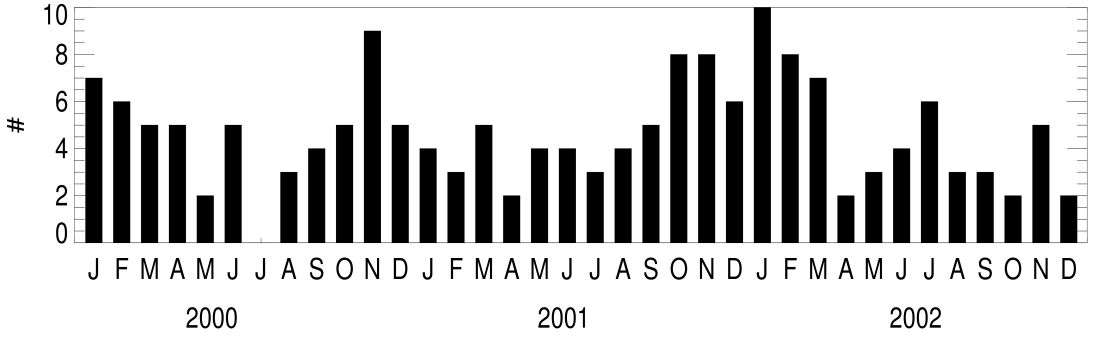

Figure 5.14: Number of frontal overpasses with the streak statistic parameter in 2000-2002 for each individual month for threshold set 1.

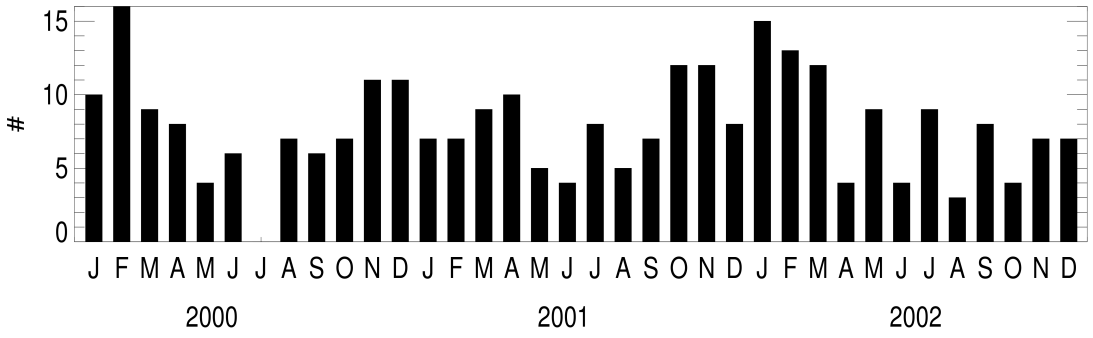

Figure 5.15: Same as Fig. 5.14, but for threshold set 2.

winter months, in summer only a few fronts go through the domain. It was expected, that the tolerant set provides results with more fronts. It includes probably also branches of frontal systems, such as cold fronts and warm fronts.

Figures 5.16 and 5.17 show zonal path, duration and zonal phase speed for the detected fronts. Note, that the zonal path as well as the duration estimated here are not always the true values of the entire life cycle of a front. The spatial range of the BALTRAD domain limits the observations of meteorological systems. Thus, while the maximal west-east path length shown in the Figs. 5.16 and 5.17 is about 1500 km, it is clearly not the case for complete frontal systems. However, the zonal speed values of fronts should estimate a climatological "truth". 167 frontal overpasses for conservative and 284 for tolerant thresholds fullfill the required threshold conditions as determined above in the observation period. The mean zonal phase speed lies for both sets at approx. 7 m/s (7.22 m/s for set 1 and 6.88 m/s for set 2). There is no seasonal dependency of zonal speed (note the colors of symbols in left panels of Fig. 5.16 and 5.17). The close agreement of the results of both threshold sets is an indice, that the introduced methods to investigate frontal overpass statistics are rather insensitive to

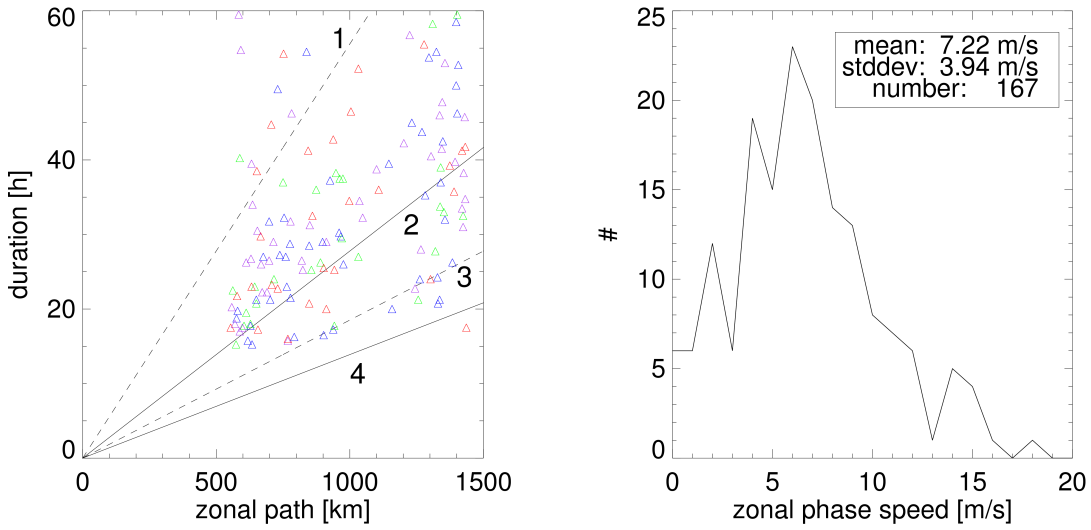

(a) (b)

Figure 5.16: Zonal path, duration and zonal phase speed of frontal systems for threshold set 1. (a) shows the duration of frontal overpasses as a function of their zonal path. The different colours indicate the season of the overpass (blue for winter (DJF); green for spring (MAM); red for summer (JJA) and purple for autumn (SON). Lines 1 to 4 are isolines of zonal phase speed (1- 5 m/s; 2- 10 m/s; 3-15 m/s; 4-20 m/s). (b) illustrates the frequency of occurrence of zonal phase speed.

subjectively choosen thresholds.

5.3 Summary of application to three years of BALTRAD data

It was found that frontal precipitation dominates the Baltic area. About two-thirds of the rainfall events were found to be frontal. The interannual variability in the investigated period was weak. However, the number of frontal overpasses depends strongly on the season. The fraction of non-frontal events in summer season (from May through September) is two to three times higher than in the cold season. This is caused by a higher frequency of frontal overpasses in autumn and spring and by differential heating above heterogeneous lake-dominated land regions in summer. This conclusion is supported by the inspection of the diurnal cycle. The convective-determined non-frontal events have a significant diurnal cycle with peaks in afternoon hours above land surfaces. This characteristic feature is particularly distinct in summer season above lake dominated regions of Finland.

During summer, rain frequencies reach levels of about 10 percent, with some periods exceeding 13 percent. The warm season is, in general, the time of convective rain and a

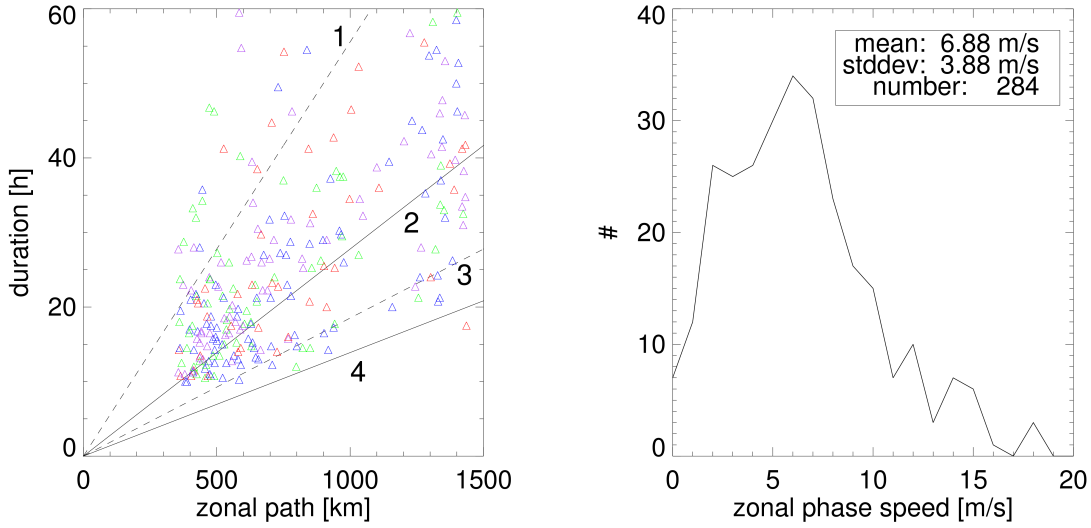

(a) (b)

Figure 5.17: Same as Fig. 5.16, but for threshold set 2.

significant diurnal cycle is noticed. Summer rainfall occurs more frequently at daytime due to an increased partition of convective rain in afternoon hours. The convective partition in summer at afternoon hours reaches peak values of more than 60 percent. These examinations were limited by the size of the radar composite images. All frontal systems may not be identified correctly, especially if a significant fraction of the frontal system does not exist within the radar range. Hence, it is likely that the frontal partition is higher than in the above presented results. This error are estimated by the author to be about 5 percent, and this potential error effects mainly the edge areas of the image domain.

The diurnal variability of all frontal events during the entire period is evanescent. This fits the expectations, because frontal overpasses might occur at any day and night hour with the same probability. However, in summer season the diurnal variability of all rain events could not be explained exclusively by convective events. Frontal precipitation has a significant diurnal cycle during the summer in some regions and daytime peaks in afternoon hours. The span of lifetime of frontal systems usually exceeds the range of a single day by multiple times. Thus, the different phases of the frontal cycle can hardly explain the observed effects and the likelihood that a frontal system lays over the region in a particular hour of the day is equal to any other hour. It is also unlikely that the overpass of individual parts of frontal systems has a diurnal cycle. In fact, it seems that the potential for precipitation during afternoon hours increases within or close to frontal systems, regardless of the phase of frontogenesis. This prevalence of frontal-related precipitation could be explained by the increased instability caused by particular temperature and moisture conditions in afternoon

hours above heated surfaces. Further investigations should divide frontal systems into subclasses, like cold fronts, warm fronts or occlusions as introduced in Tetzlaff and Hagemann (1986) and could confirm this hypothesis.

The period of three years is also too short and the variability of the number of frontal overpasses are too high to characterise this investigation as a climatology. Long-term investigations could provide better analyses of any trends.